Supplementary Information

Structure-property relationship of donor-acceptor acridones – An optical, electrochemical and computational study

Thériault, K. D.; Radford, C. L.; Parvez, M.; Heyne, B.; Sutherland, T. C.
University of Calgary, Department of Chemistry
2500 University Dr. NW
Calgary, Alberta, Canada
T2N 1N4
todd.sutherland@ucalgary.ca

Contents:

S1) FTIR spectra
1

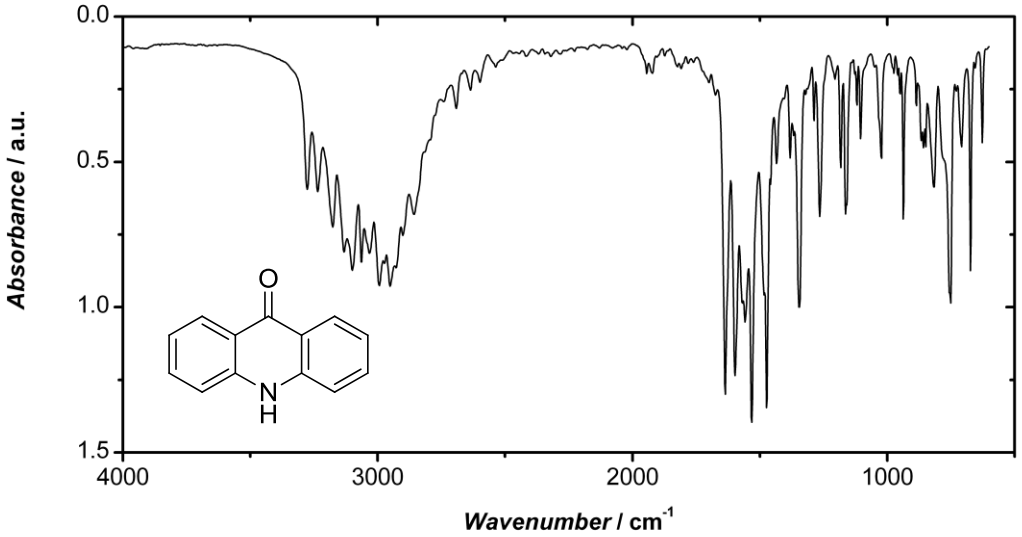

2a

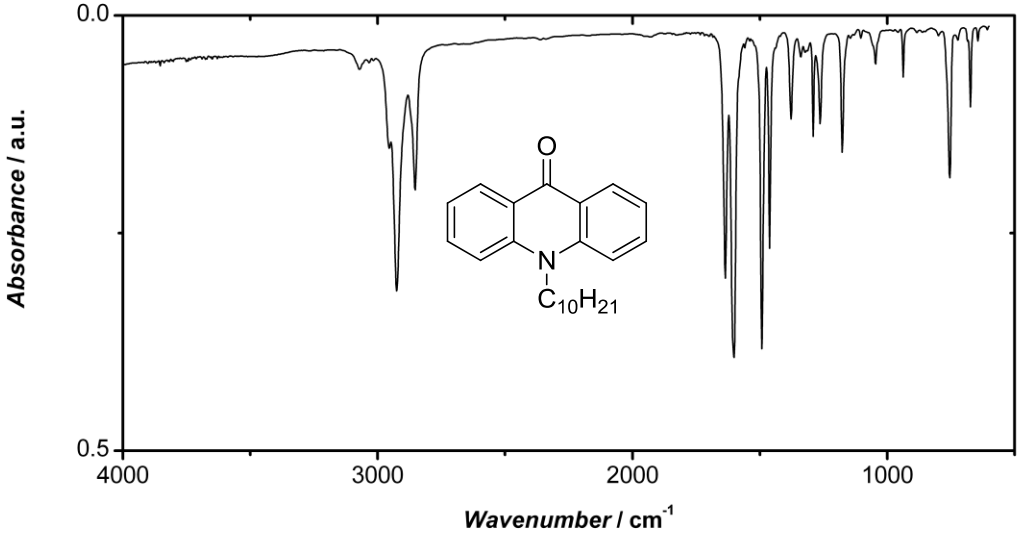

2b

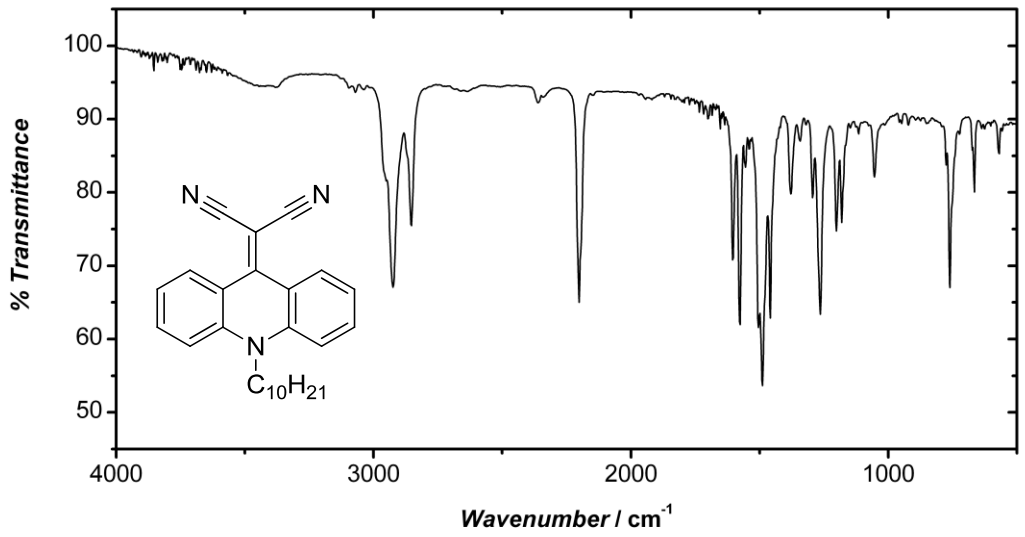
% Transmittance
100
90
80
70
60
50
4000
3000
2000
1000
Wavenumber / cm-1
N
N
N
C10H21

3a

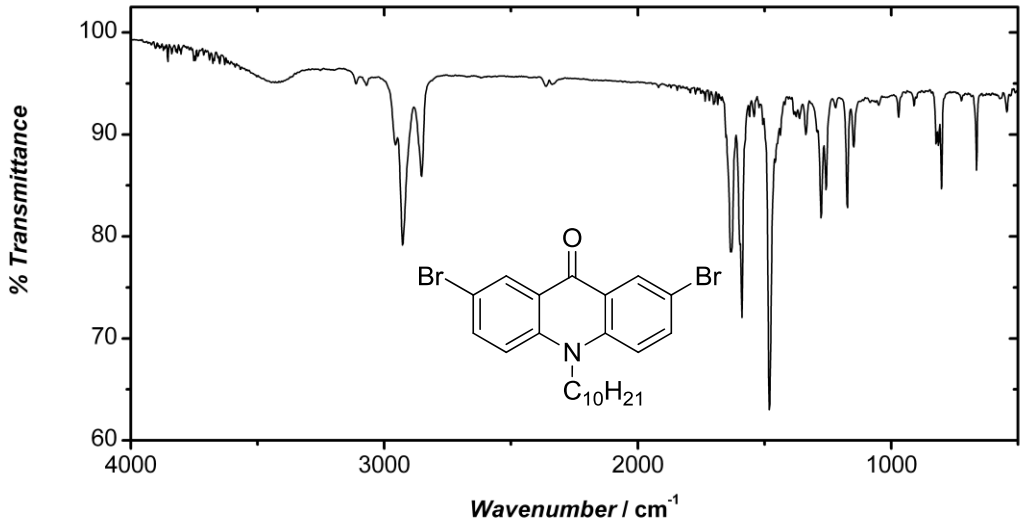
% Transmittance
100
90
80
70
60
4000
3000
2000
1000
Wavenumber / cm-1
O
Br
Br
N
C10H21

3b

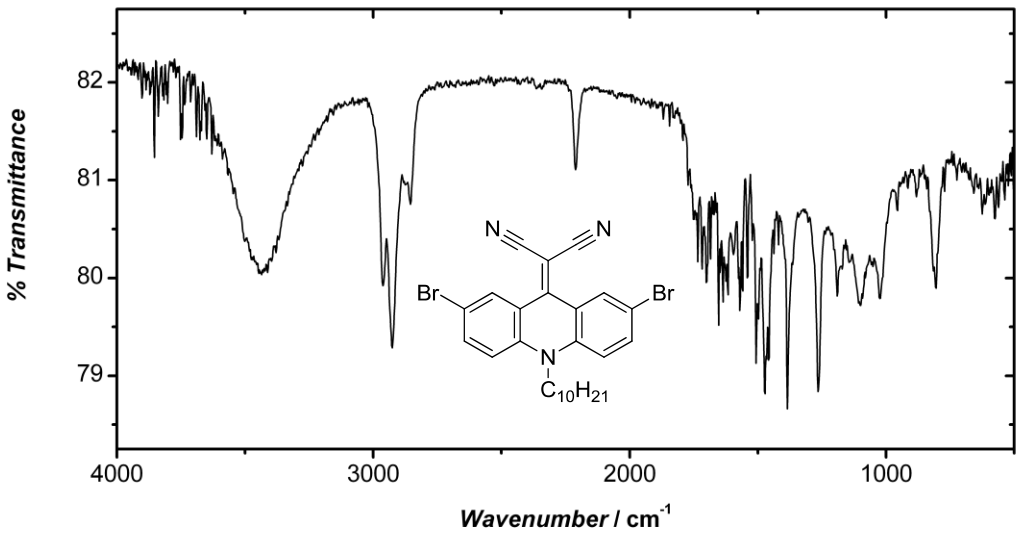
% Transmittance
82
81
80
79
4000
3000
2000
1000
Wavenumber / cm-1
N
N
Br
Br
N
C10H21

4a

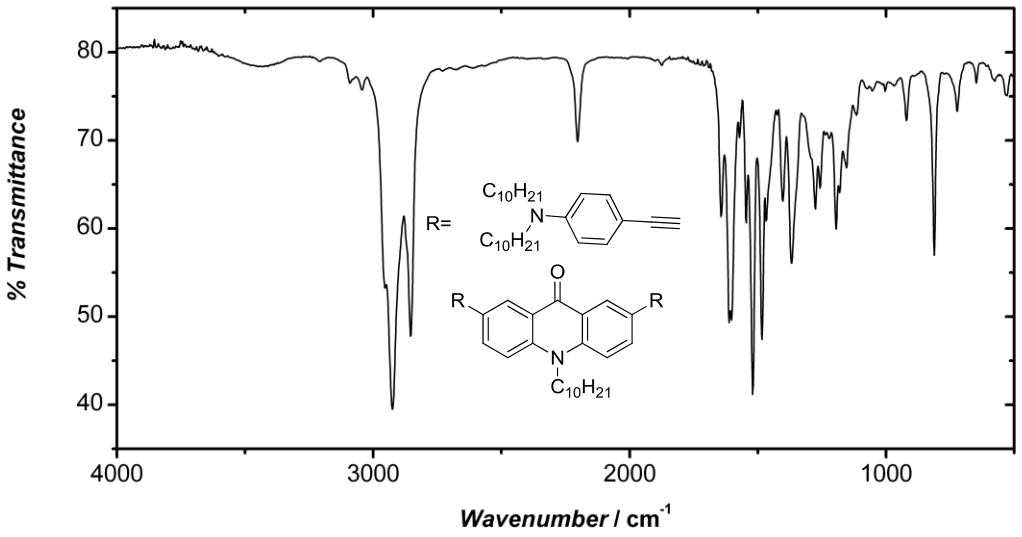
% Transmittance
80
70
60
50
40
4000
3000
2000
1000
Wavenumber / cm-1
R=
C10H21
N
C10H21
O
R
R
N
C10H21

4b

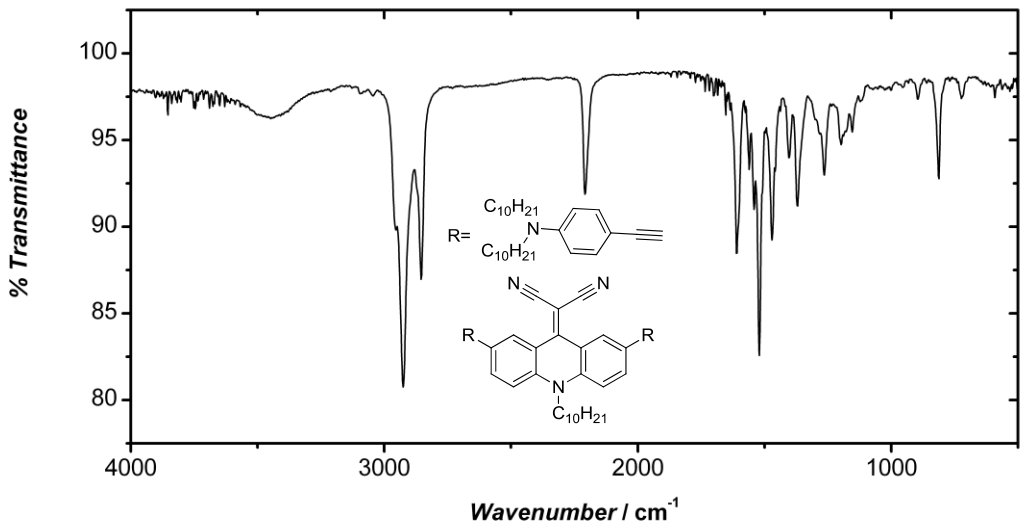

Figure S1: FTIR spectra of **1, 2a, 2b, 3a, 3b. 4a and 4b** on ground KBr.

Cyclic Voltammetry

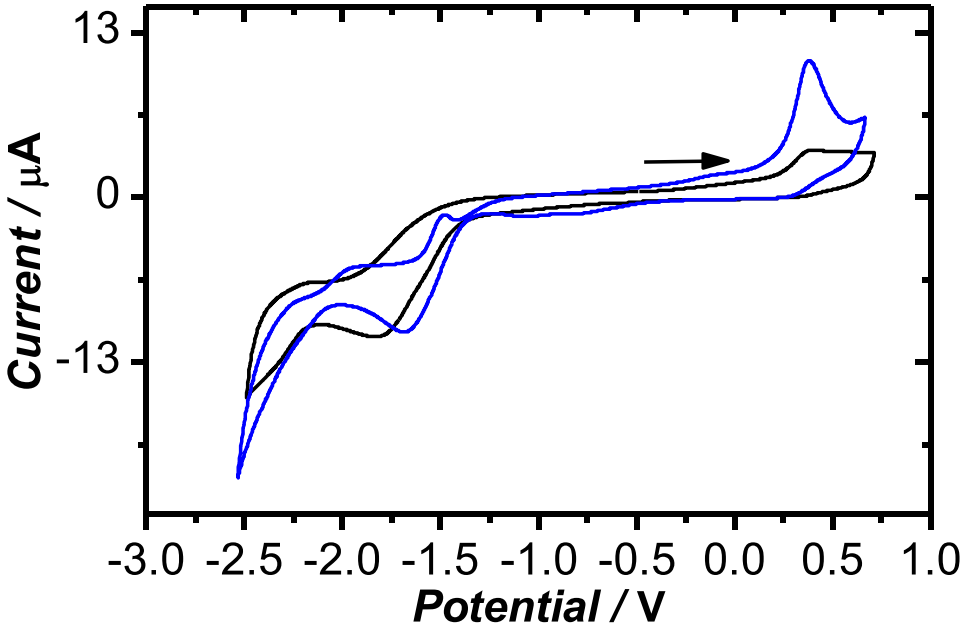

Figure S2: Cyclic voltammetry of **4a** (black) and **4b** (blue) in DCM vs Fc/Fc^+.

Differential Pulse Voltammetry

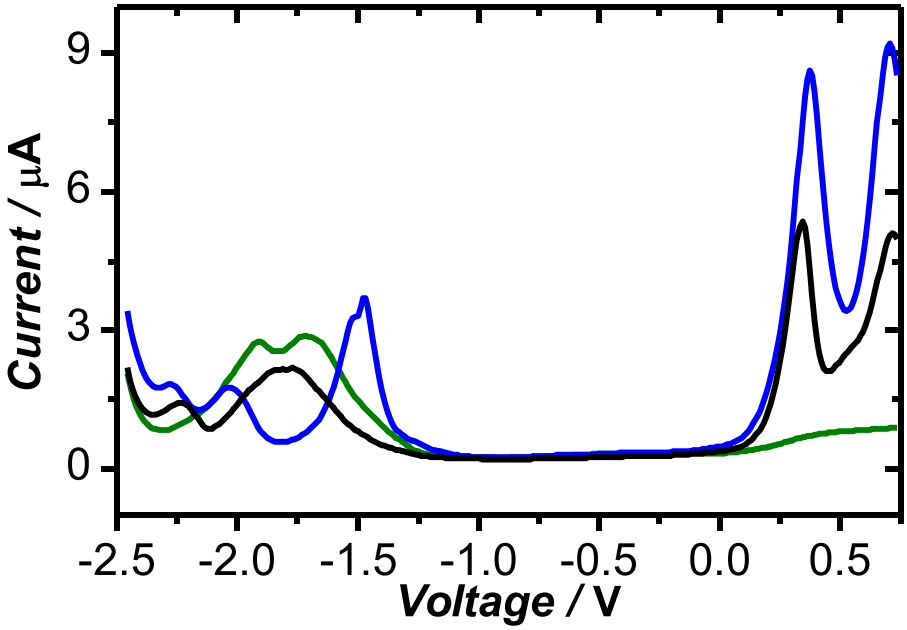

Figure S3: Differential Pulse Voltammetry of **4a** (black), **4b** (blue), and the blank solvent and electrolyte (green) in DCM vs Fc/Fc^{+}.

UV-Vis Spectroelectrochemistry

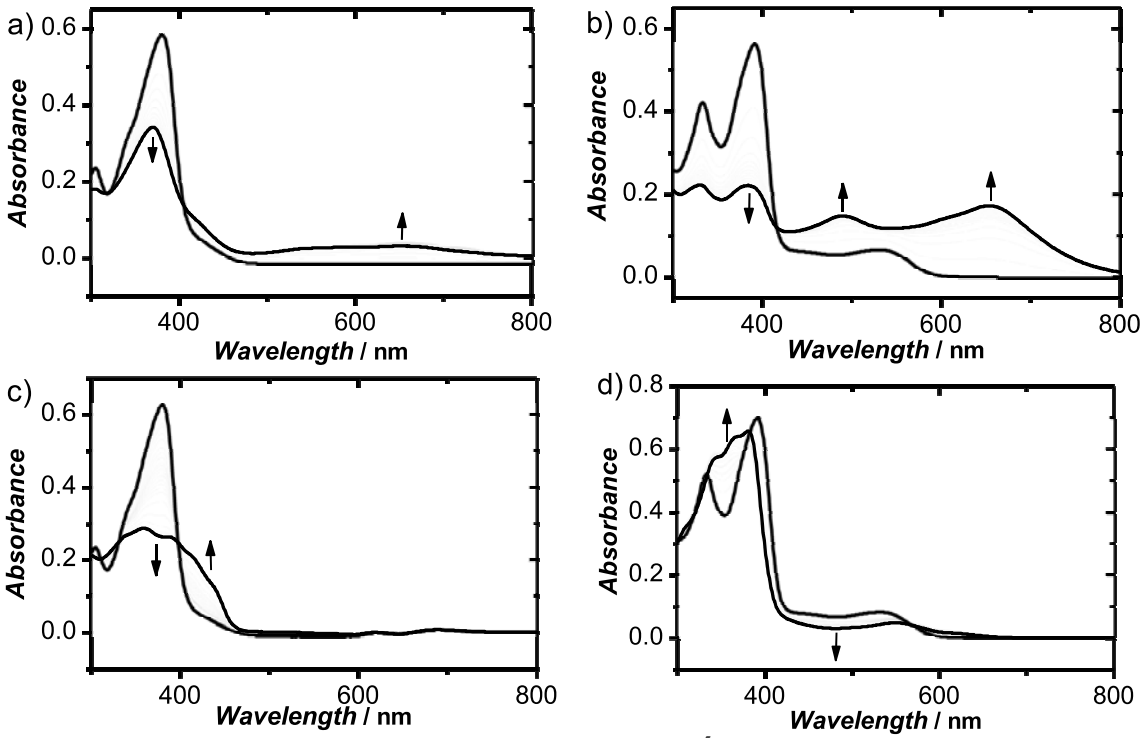

Figure S4: UV-Vis of **4a** (left) and **4b** (right) in DCM at 10^{-5} M with 0.1 M tetrabutylammonium tetrafluoroborate, with an applied oxidative a) 0.7 V b) 0.9 V and reductive c) -1.5 V d) -1.0 V potential recorded once a minute. The initial and final spectra are shown in black.

FTIR Spectroelectrochemistry

Using the spectroelectrochemical cell, oxidation and reduction reactions were investigated by FT-IR, as shown in Figure 7. For clarity purposes, the solution IR spectra of the neutral species, **4a** and **4b**, in the presence of electrolyte, [nBu$_4$N][PF$_6$], were collected prior to applying a potential and are shown as the top panels of Figure S5. Upon application of either the reductive or oxidative potentials, successive FT-IR scans were recorded at 1-minute time intervals and displayed as transmission difference ($\Delta\%T$) spectra in the bottom panels of Figure S5. Thus, upward peaks in the transmission difference spectra indicate consumption of neutral compound and downward signals indicate the growth of new IR-active modes of the charged species.

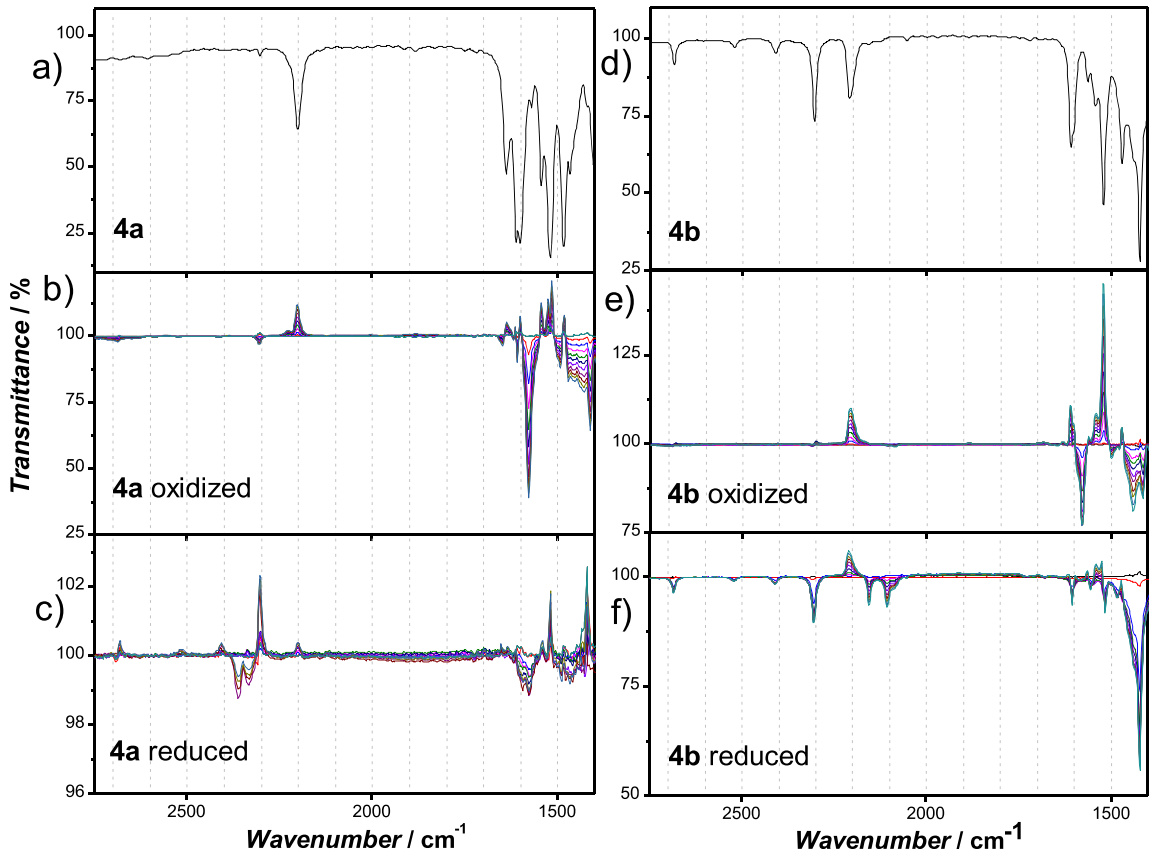

Figure S5: Solution transmission FT-IR spectra of **4a** and **4b** in the top two panels. During either oxidative or reductive applied potentials, the change in transmission intensity are shown as the lower panels in DCM at 1 mM compound and 0.01 M tetrabutylammonium tetrafluoroborate electrolyte.

Solvatochromism

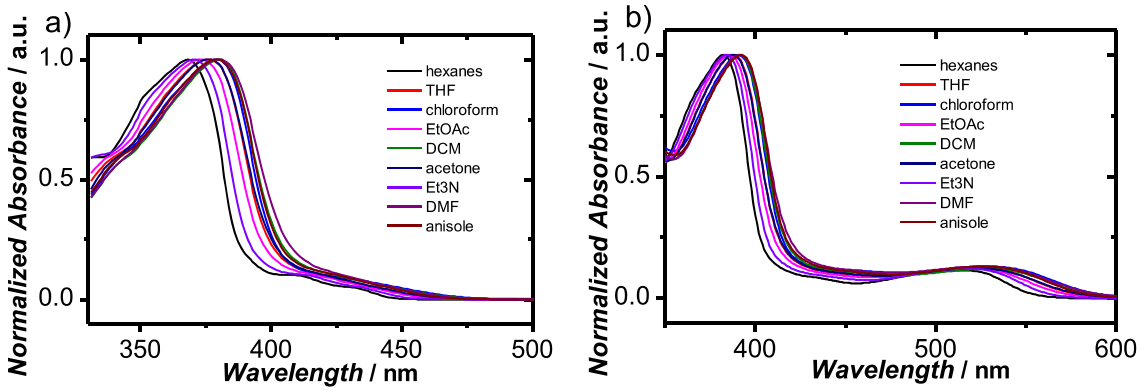

Figure S6: UV-Vis spectra of a) **4a** b) **4b** in solvents of varying polarity.

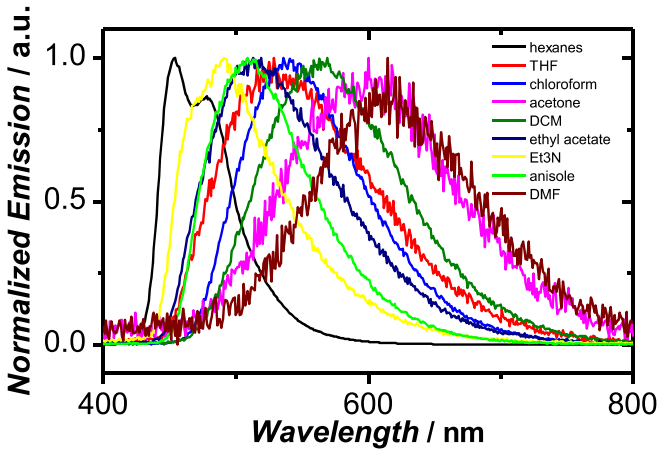

Figure S7: Emission spectra of **4a** in solvents of varying polarity.

Solvent Analysis

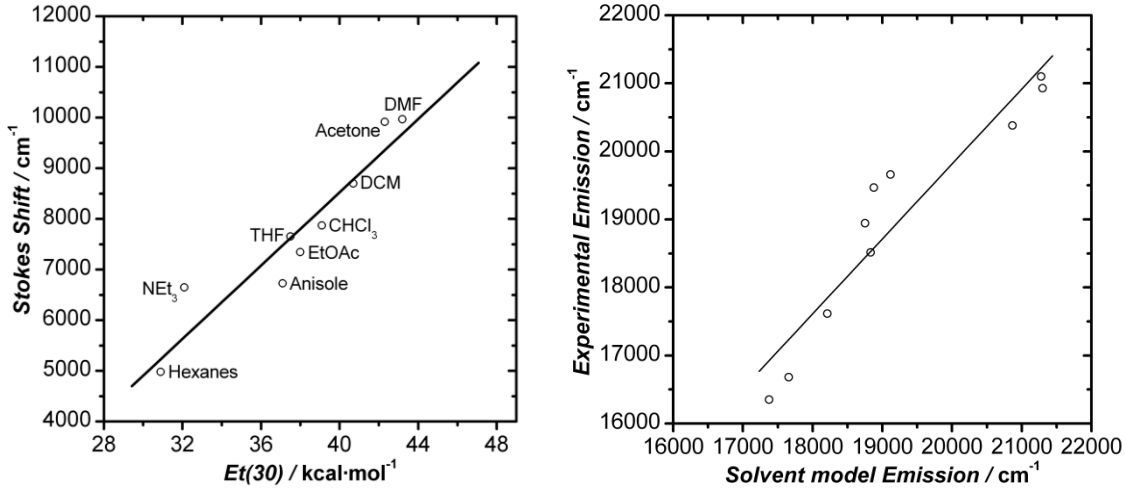

Figure S8: Solvent analysis of **4a**, plotted as stokes shift vs. $E_T(30)$ solvent value (left) and experimental vs. calculated emission using a solvent model based on Catalan[1] (right).

Crystal Packing

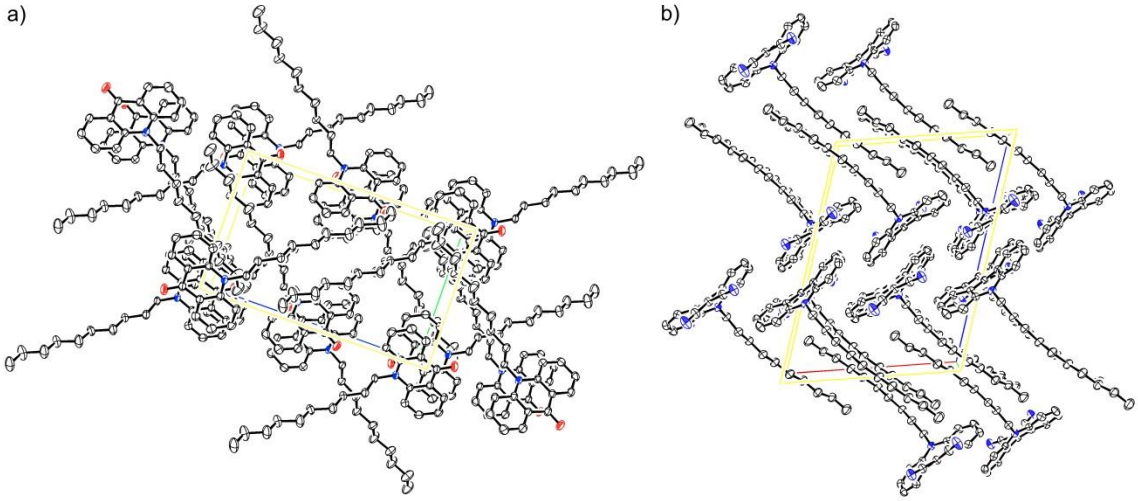

Figure S9: Ortep representation of the packing motif of a) 2a and b) 2b with ellipsoids shown at 50% probability. Hydrogens have been removed for clarity and atoms are color coded as follows (carbon = black, nitrogen = blue, oxygen = red).

Calculation Results

Table S1: Optical transitions of all calculated charged species of **4a** and **4b** shown with the involved molecular orbitals

	Wavelength / nm	Transition Coefficient	Oscillator Strength	Ground State Orbital		Excited State Orbital
4a neutral	451	0.99	0.14	HOMO -1 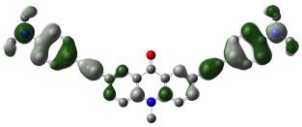	→	LUMO 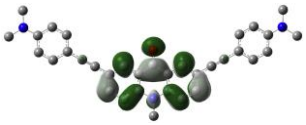
	412	0.96	2.16	HOMO 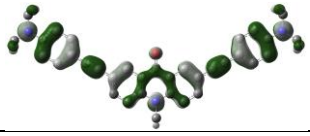	→	LUMO+1 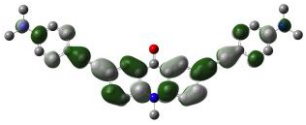
4a 1+	2802	0.93[a]	0.73	HOMO-1 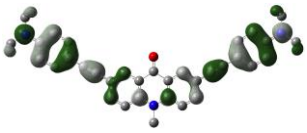	→	SOMO 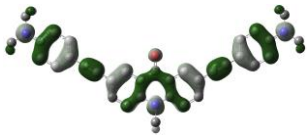
	1053	1.00[a]	0.11	HOMO-2 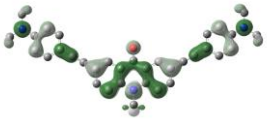	→	SOMO 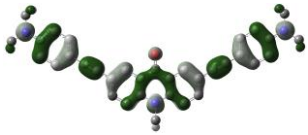
	687	1.00[a]	0.15	HOMO-3 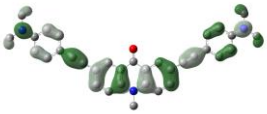	→	SOMO 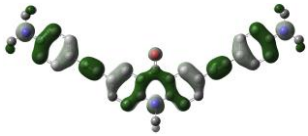
4a 2+	1492	0.78[a]	1.60	HOMO 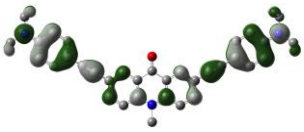	→	LUMO 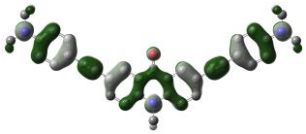

	760	0.93[a]	0.21	HOMO-1 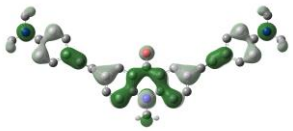	→	LUMO 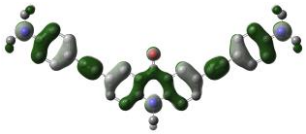
	587	0.97[a]	0.44	HOMO-2 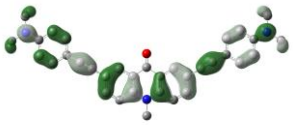	→	LUMO 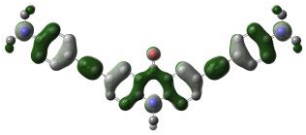
4a 1-	705	0.90[a]	0.36	SOMO 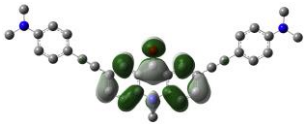	→	LUMO+4 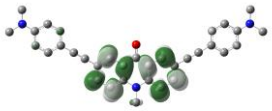
4a 2-	3038	0.99	0.013	HOMO 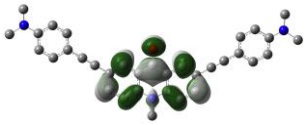	→	LUMO 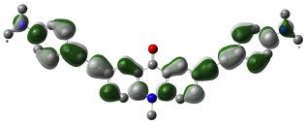
	1669	1.00	0.015	HOMO 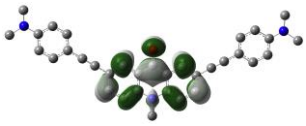	→	LUMO+1 
	1175	1.00	0.010	HOMO 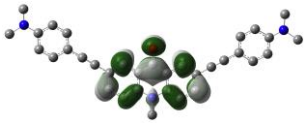	→	LUMO+2 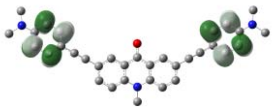
	850	0.93	0.006	HOMO 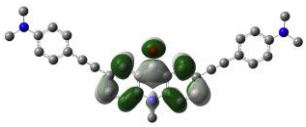	→	LUMO+4 
4b neutral	590	0.99	0.16	HOMO-1 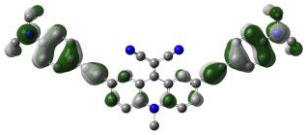	→	LUMO 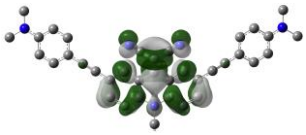

	419	0.96	1.81	HOMO 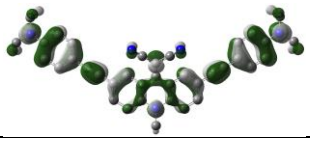	→	LUMO+1 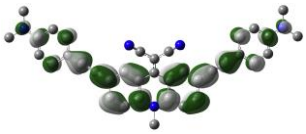
4b 1+	3026	0.89[a]	0.60	HOMO-1 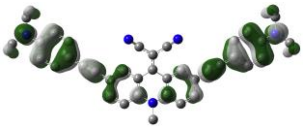	→	SOMO 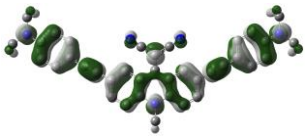
	1120	1.00[a]	0.11	HOMO-2 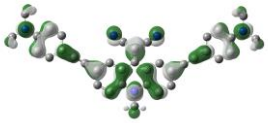	→	SOMO 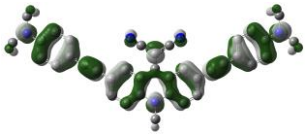
	694	0.94[a]	0.10	HOMO-1 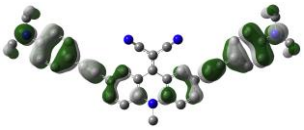	→	LUMO 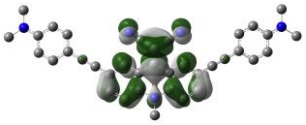
	687	0.95[a]	0.11	HOMO-3 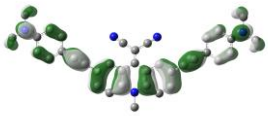	→	SOMO 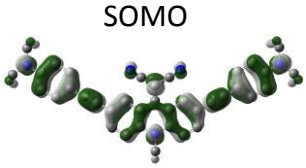
4b 2+	1548	0.78[a]	1.36	HOMO 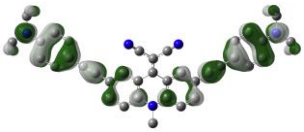	→	LUMO 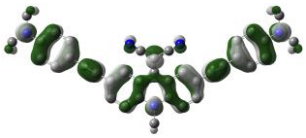
	817	0.94[a]	0.21	HOMO-1 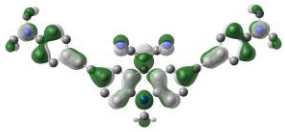	→	LUMO 
	614	1.00[a]	0.30	HOMO 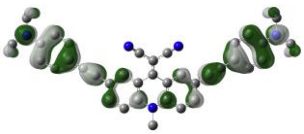	→	LUMO+1 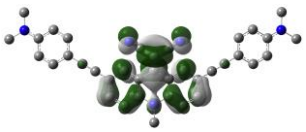
	589	0.97[a]	0.43	HOMO 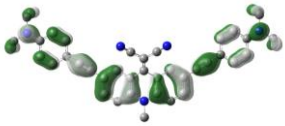	→	LUMO 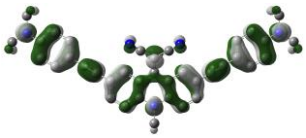

				SOMO		LUMO
4b 1-	796	0.99[a]	0.04	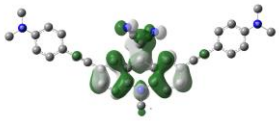	→	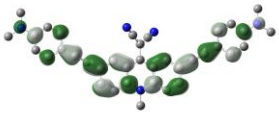
				HOMO-1		SOMO
	652	0.85[a]	0.03	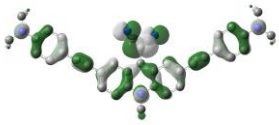	→	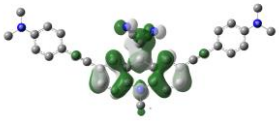
				SOMO		LUMO+1
	580	0.81[a]	0.04	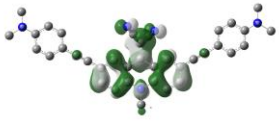	→	
				SOMO		LUMO+2
	511	0.67[a]	0.20	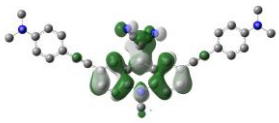	→	
				HOMO-2		SOMO
	500	0.39[a]	0.06		→	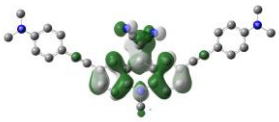
				HOMO		LUMO
4b 2-	887	0.98	0.05		→	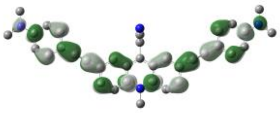

			HOMO		LUMO+1
690	0.99	0.05		→	
			HOMO		LUMO+4
483	0.78	0.10		→	

a) Transition coefficients of the 1+, 2+ and 1- species were calculated by normalizing the sum of the squares of all transitions of the excitation in question, as described by Vogt *et. al.*[2]

Table S2: Calculated IR frequencies

	C≡C sym / cm^{-1}	C≡C anti / cm^{-1}	C=O / cm^{-1}	C≡N sym / cm^{-1}	C≡N anti / cm^{-1}	C=C of malono / cm^{-1}
4a (2-)	2171 (m)	2166 (s)	1348 (w)			
4a (1-)	2184 (w)	2182 (m)	1429 (m)			
4a	2190 (m)	2190 (s)	1566 (s)			
4a (1+)	2154 (w)	2112 (s)	1619 (w)			
4a (2+)	2125 (w)	2095 (s)	1644 (w)			
4b (2-)	2180 (w)	2179 (m)		2120 (m)	2027 (s)	N/A
4b (1-)	2189 (w)	2189 (w)		2146 (m)	2184 (s)	N/A
4b	2190 (w)	2190 (s)		2210 (m)	2191 (w)	1439 (s)
4b (1+)	2154 (w)	2119 (s)		2220 (w)	2204 (w)	1457 (w)
4b (2+)	2125 (w)	2099 (s)		2232 (w)	2217 (w)	1484 (w)

(B3LYP/6-31+g(d) basis set) corrected using 0.96 correction factor, green represents neutral species, blue represents lower frequencies than the neutral species and red represents higher frequencies than the neutral species. Relative signal intensities marked as s = strong, m = medium and w = weak. Weak signals may not be observable experimentally.

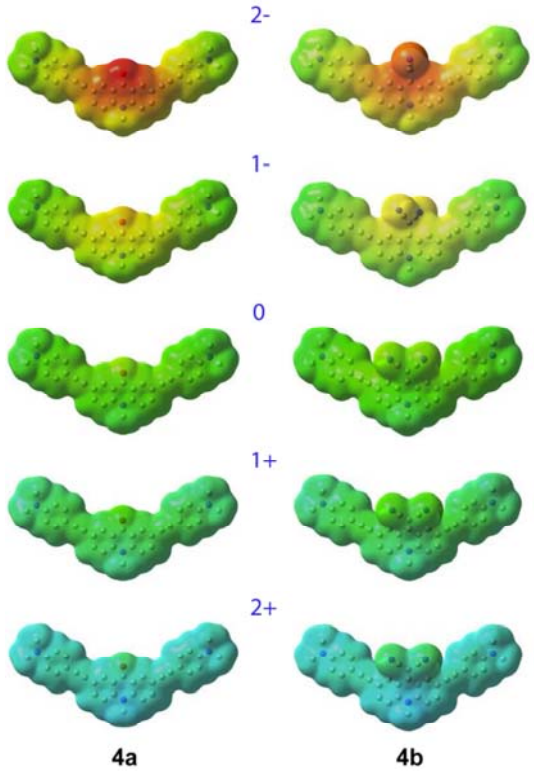

Figure S10: Electron density calculations of **4a** (left) and **4b** (right) in different oxidation states (blue number). Blue to red areas representing regions of low to high electron density, respectively.

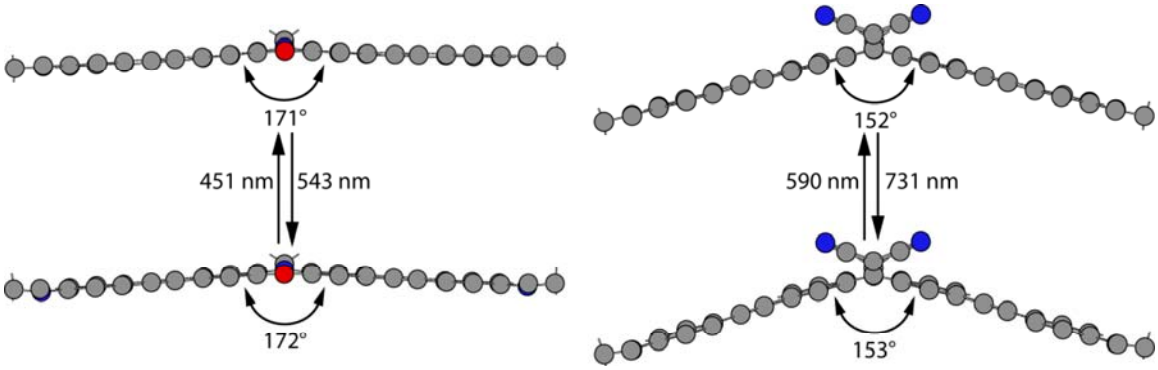

Figure S11: Optimized structures calculated for the ground state (bottom) and excited state (top) of **4a** (left) and **4b** (right) with corresponding calculated absorption and emission wavelengths (B3LYP/6-31+g(d))

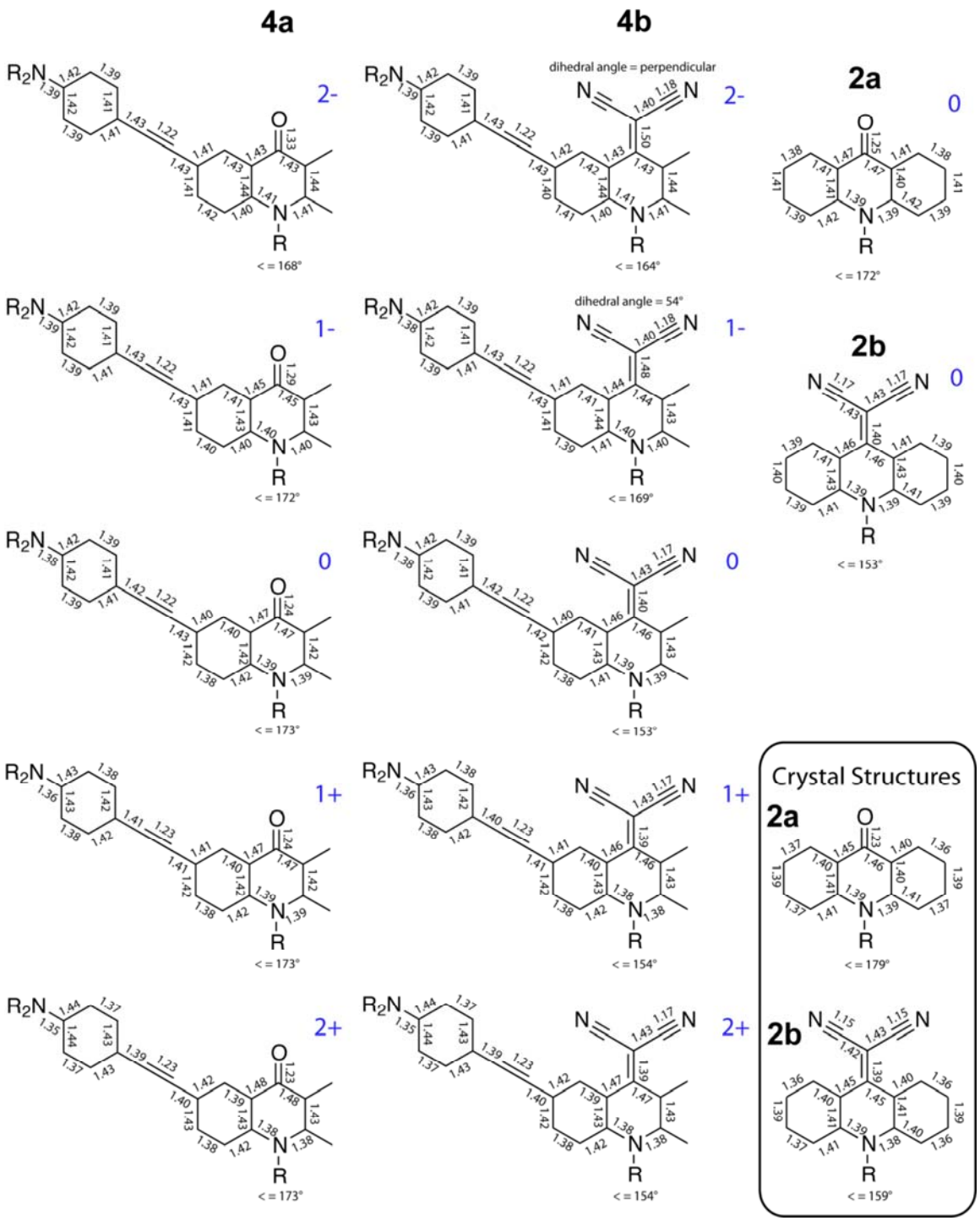

Figure S12: Selected bond length and angle between benzo rings of optimized structures (B3LYP/6-31+g(d)) of charged and neutral species discussed in this report. The angles below the structures, labelled as "<" are the angle between annulated benzo rings. The angles above select structures indicate the dihedral angle between the plane of the malononitrile functional groups vs. the plane of the molecule when twisted out of plane. Crystal structures are shown in the box for comparison.

NMR Spectra

2a

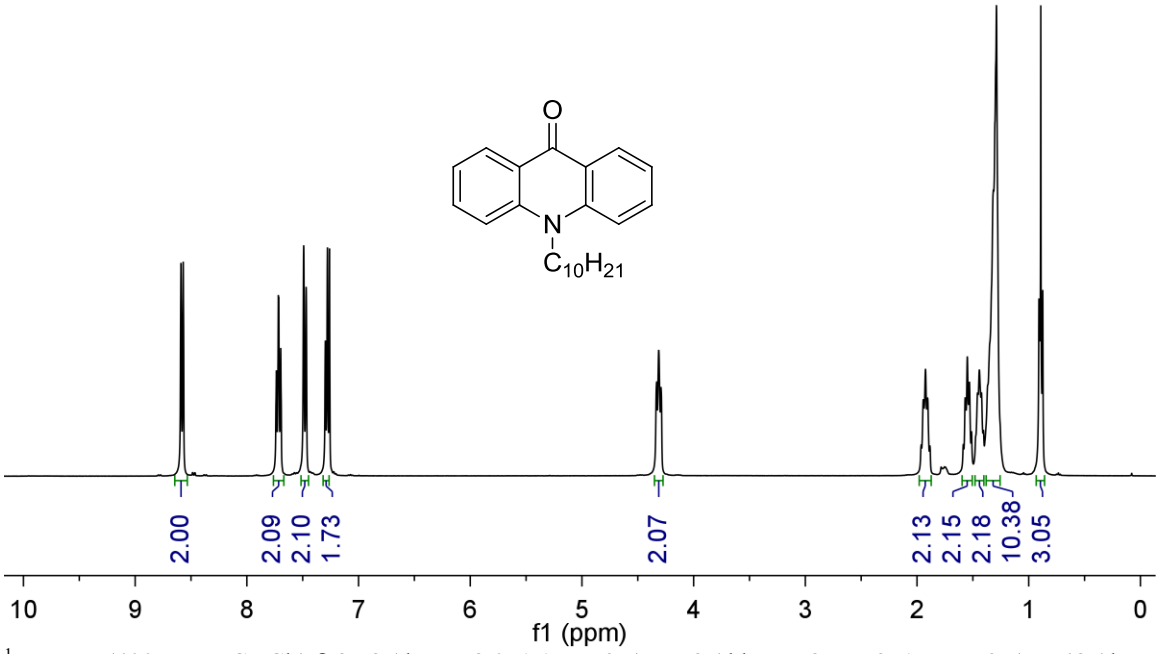

^{1}H NMR (400 MHz, $CDCl_3$) δ 8.58 (dt, *J* = 8.0, 1.1 Hz, 2H), 7.72 (ddt, *J* = 8.5, 7.2, 1.5 Hz, 2H), 7.48 (d, *J* = 8.7 Hz, 2H), 7.29 (d, *J* = 7.4 Hz, 2H), 4.37 – 4.27 (m, 2H), 1.99 – 1.86 (m, 2H), 1.55 (p, *J* = 7.1 Hz, 2H), 1.44 (p, *J* = 6.6 Hz, 2H), 1.39 – 1.24 (m, 10H), 0.89 (t, *J* = 7.0 Hz, 3H).

2a

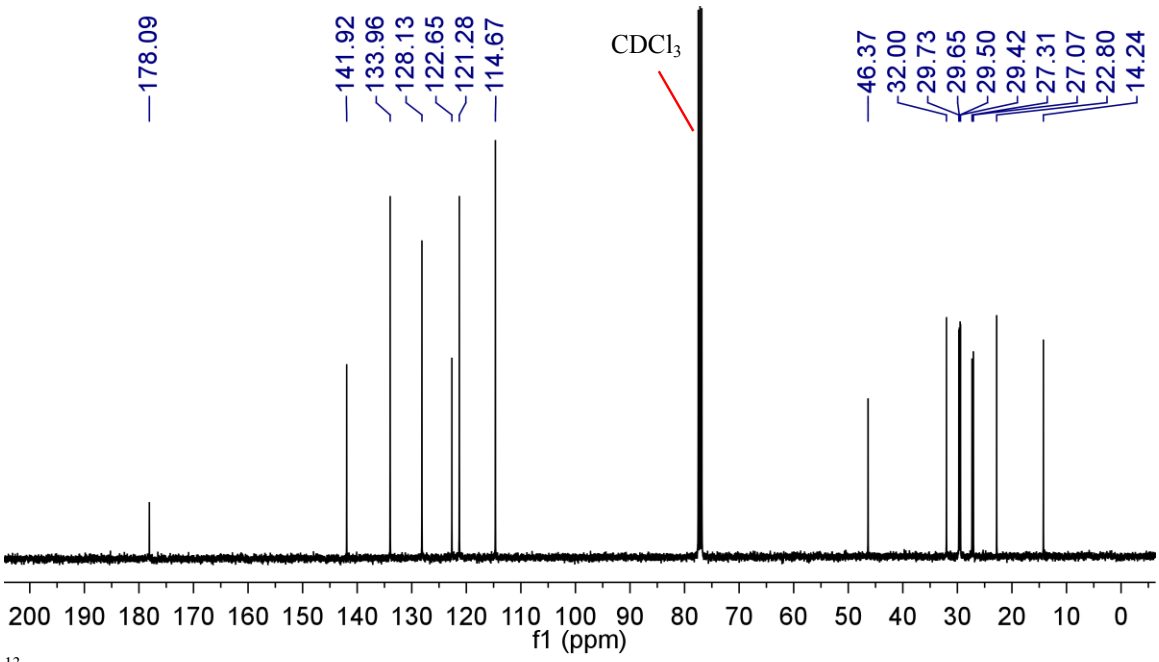

^{13}C NMR (101 MHz, $CDCl_3$) δ 178.09, 141.92, 133.96, 128.13, 122.65, 121.28, 114.67, 46.37, 32.00, 29.73, 29.65, 29.50, 29.42, 27.31, 27.07, 22.80, 14.24.

2b

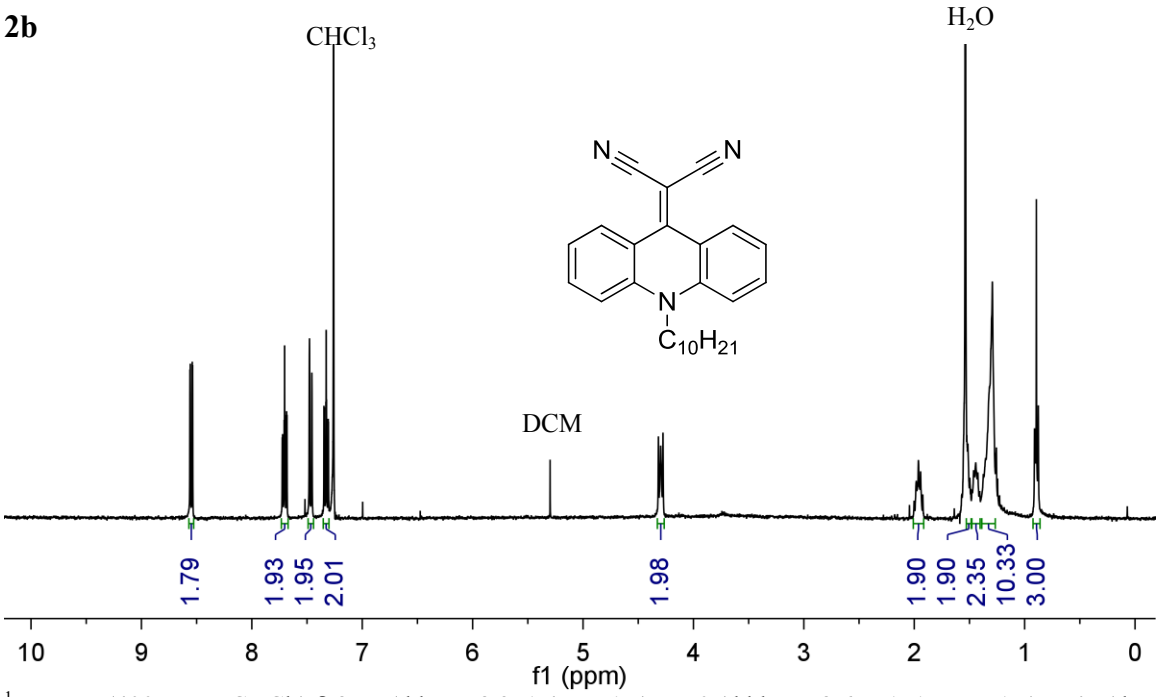

^{1}H NMR (400 MHz, $CDCl_3$) δ 8.55 (dd, *J* = 8.3, 1.4 Hz, 1H), 7.70 (ddd, *J* = 8.6, 7.1, 1.5 Hz, 1H), 7.47 (d, *J* = 8.4 Hz, 1H), 7.33 (ddd, *J* = 8.2, 7.1, 1.0 Hz, 1H), 4.44 – 4.21 (m, 1H), 1.96 (p, *J* = 7.9 Hz, 1H), 1.54 – 1.49 (m, 0H), 1.49 – 1.40 (m, 1H), 1.39 – 1.22 (m, 4H), 0.89 (t, *J* = 7.0 Hz, 1H).

2b

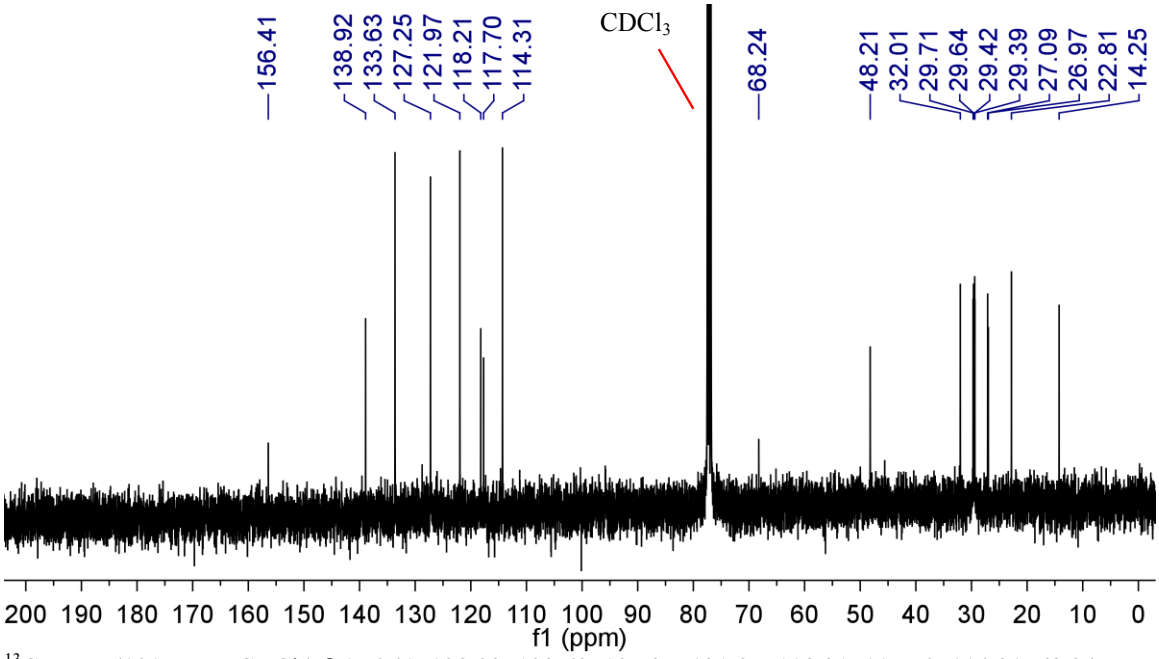

^{13}C NMR (101 MHz, $CDCl_3$) δ 156.41, 138.92, 133.63, 127.25, 121.97, 118.21, 117.70, 114.31, 68.24, 48.21, 32.01, 29.71, 29.64, 29.42, 29.39, 27.09, 26.97, 22.81, 14.25.

3a

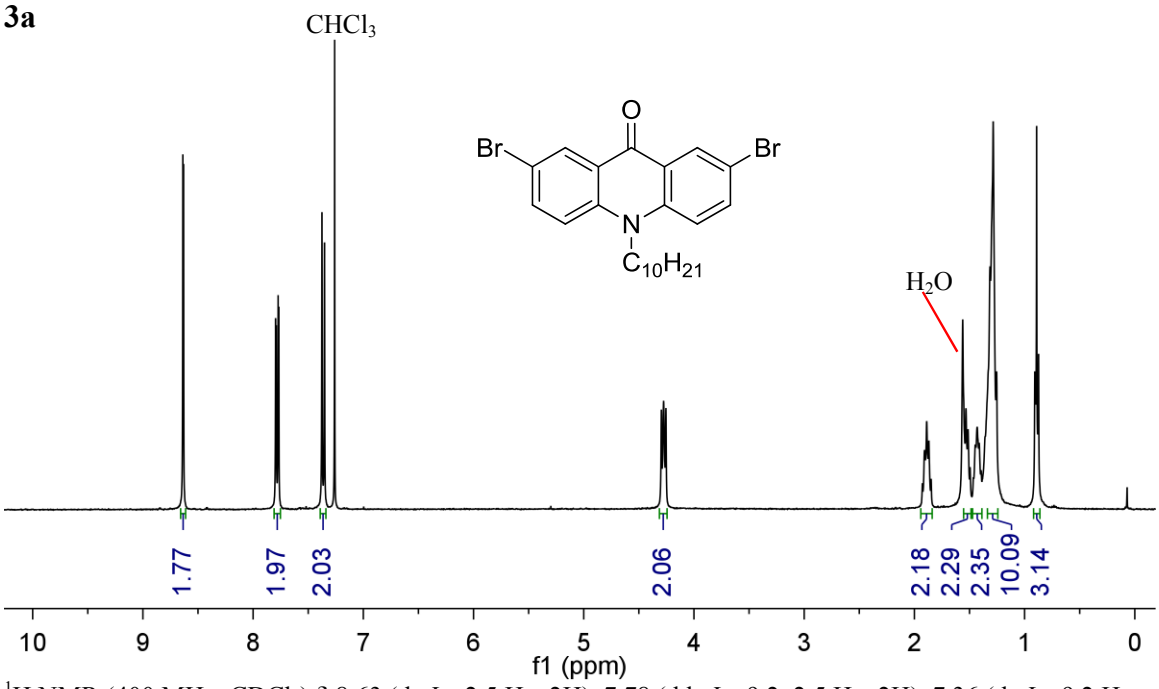

^{1}H NMR (400 MHz, $CDCl_3$) δ 8.63 (d, J = 2.5 Hz, 2H), 7.78 (dd, J = 9.2, 2.5 Hz, 2H), 7.36 (d, J = 9.2 Hz, 2H), 4.36 – 4.19 (m, 2H), 1.89 (p, J = 8.2 Hz, 2H), 1.58 – 1.48 (m, 2H), 1.49 – 1.37 (m, 2H), 1.35 – 1.21 (m, 10H), 0.89 (t, J = 6.8 Hz, 3H).

3a

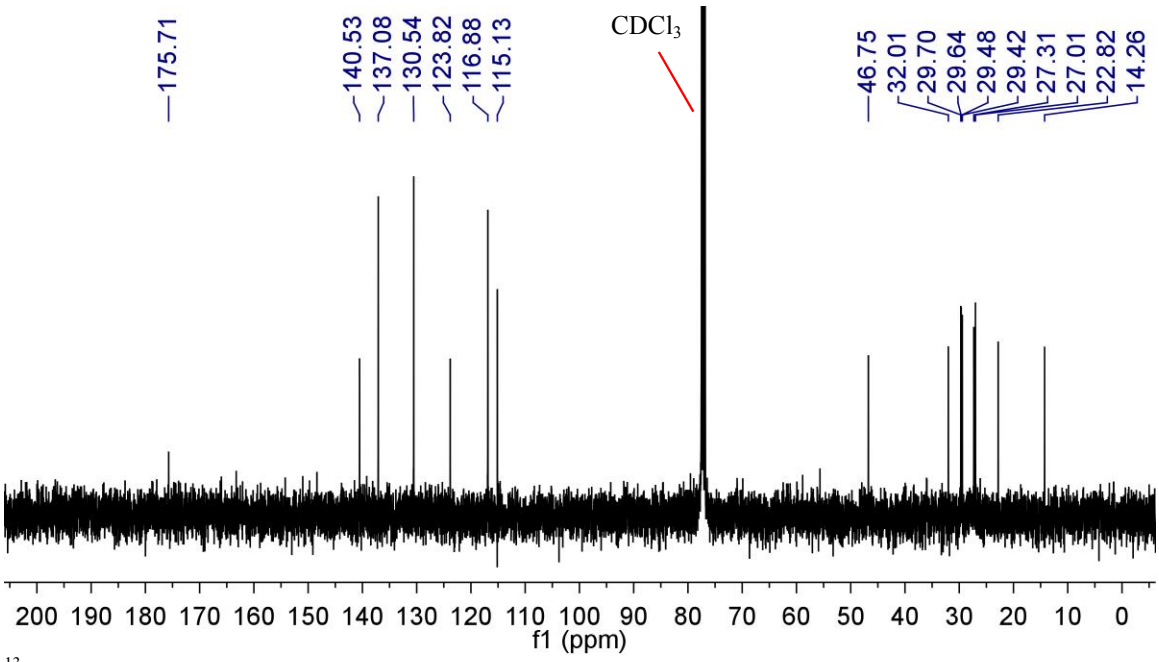

^{13}C NMR (101 MHz, $CDCl_3$) δ 175.71, 140.53, 137.08, 130.54, 123.82, 116.88, 115.13, 46.75, 32.01, 29.70, 29.64, 29.48, 29.42, 27.31, 27.01, 22.82, 14.26.

3b

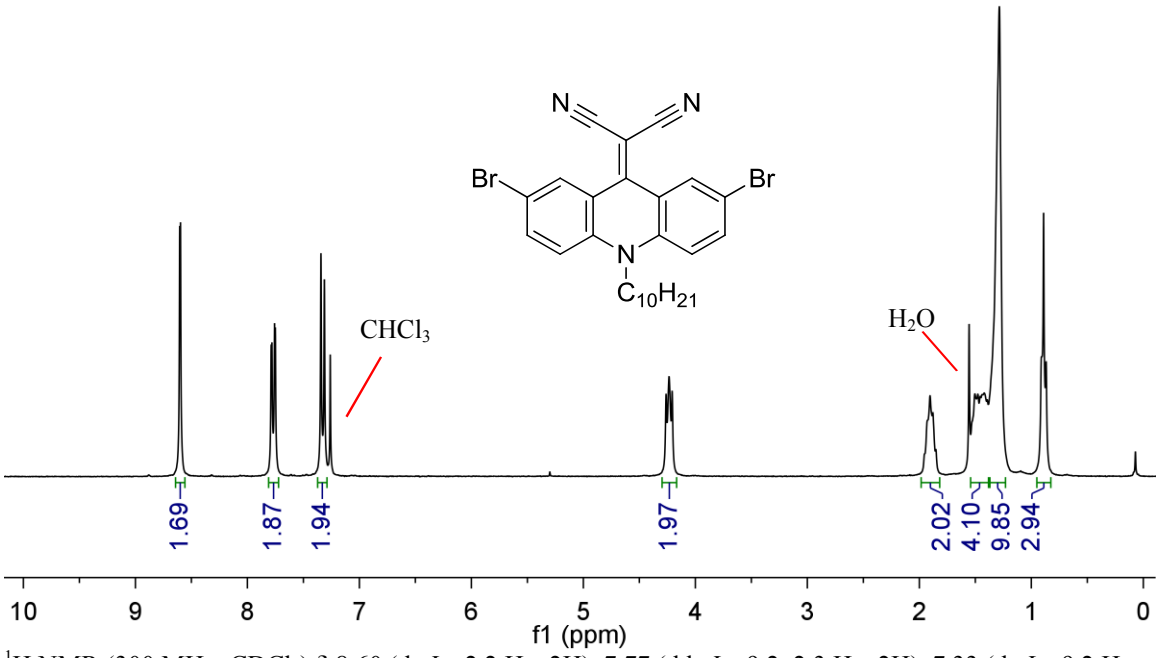

^{1}H NMR (300 MHz, $CDCl_3$) δ 8.60 (d, J = 2.2 Hz, 2H), 7.77 (dd, J = 9.2, 2.3 Hz, 2H), 7.33 (d, J = 9.2 Hz, 2H), 4.41 – 4.08 (m, 2H), 1.90 (p, J = 7.6 Hz, 2H), 1.53 – 1.38 (m, 4H), 1.38 – 1.17 (m, 10H), 0.89 (t, J = 6.3 Hz, 3H).

3b

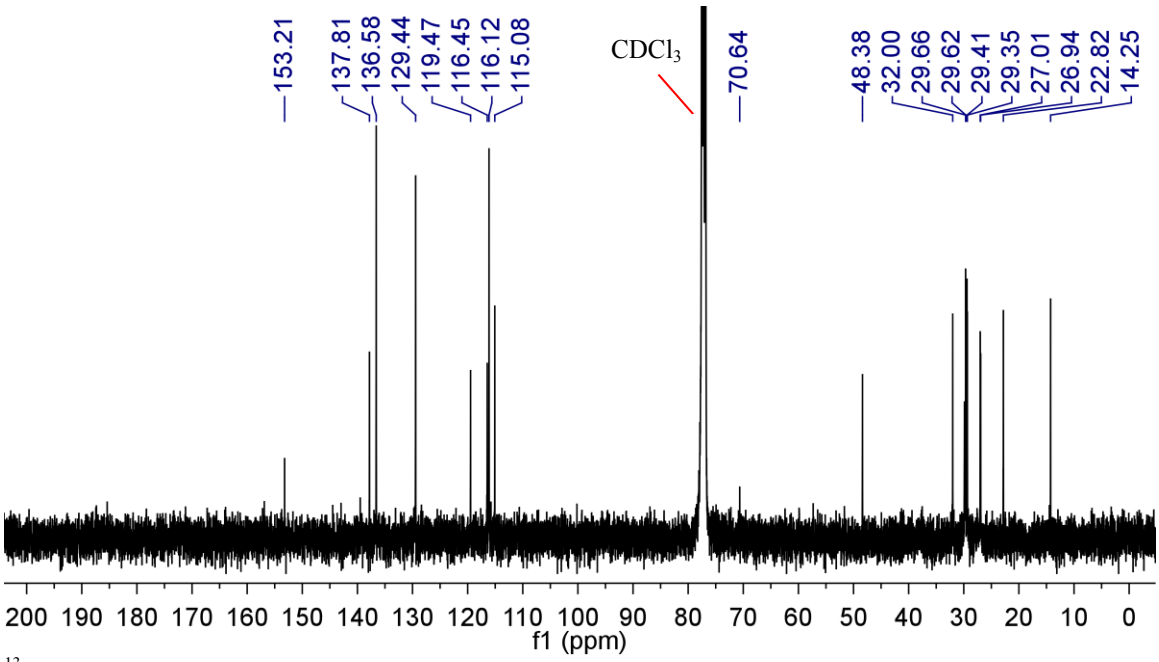

^{13}C NMR (101 MHz, $CDCl_3$) δ 153.21, 137.81, 136.58, 129.44, 119.47, 116.45, 116.12, 115.08, 70.64, 48.38, 32.00, 29.66, 29.62, 29.41, 29.35, 27.01, 26.94, 22.82, 14.25.

4a

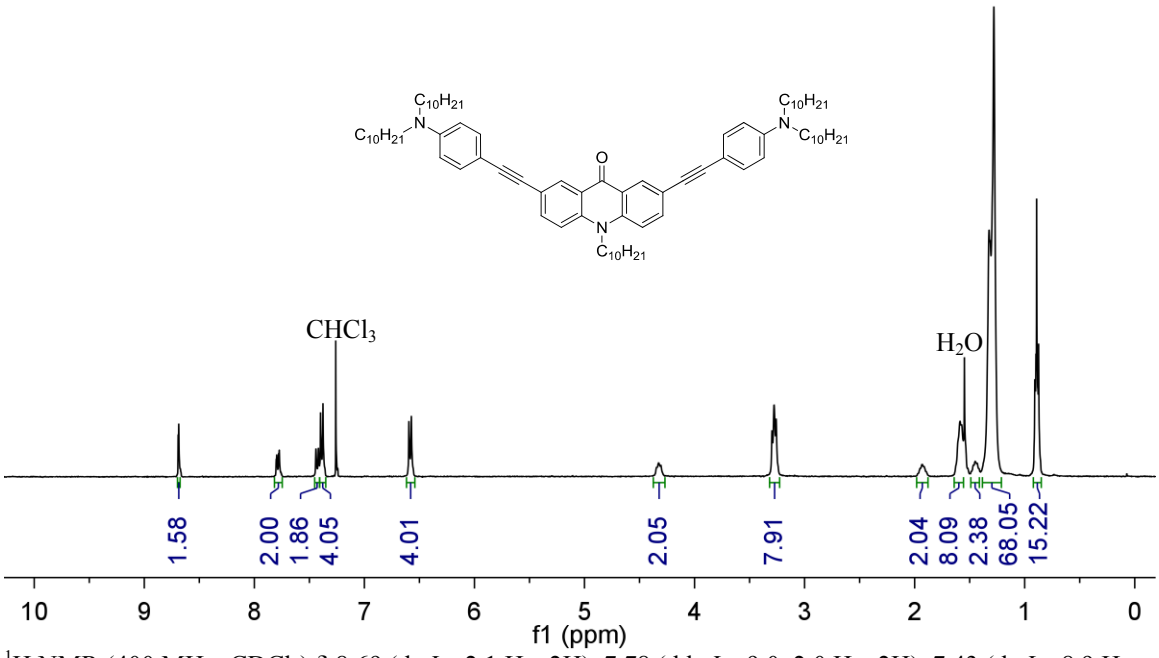

^{1}H NMR (400 MHz, $CDCl_3$) δ 8.69 (d, *J* = 2.1 Hz, 2H), 7.78 (dd, *J* = 9.0, 2.0 Hz, 2H), 7.43 (d, *J* = 8.9 Hz, 2H), 7.39 (d, *J* = 8.9 Hz, 4H), 6.58 (d, *J* = 8.9 Hz, 4H), 4.38 – 4.27 (m, 2H), 3.35 – 3.24 (m, 8H), 1.93 (p, *J* = 7.3 Hz, 2H), 1.63 – 1.56 (m, 8H), 1.50 – 1.39 (m, 2H), 1.35 – 1.22 (m, 68H), 0.96 – 0.85 (m, 15H).

4a

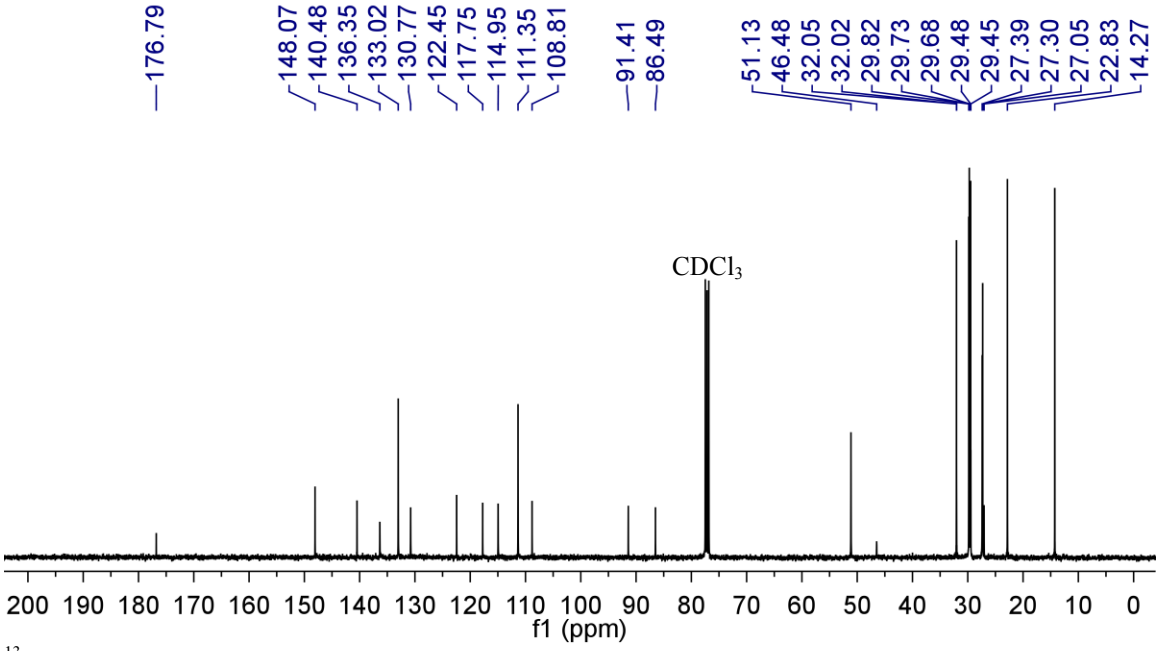

^{13}C NMR (101 MHz, $CDCl_3$) δ 176.79, 148.07, 140.48, 136.35, 133.02, 130.77, 122.45, 117.75, 114.95, 111.35, 108.81, 91.41, 86.49, 51.13, 46.48, 32.05, 32.02, 29.82, 29.73, 29.68, 29.48, 29.45, 27.39, 27.30, 27.05, 22.83, 14.27.

4b

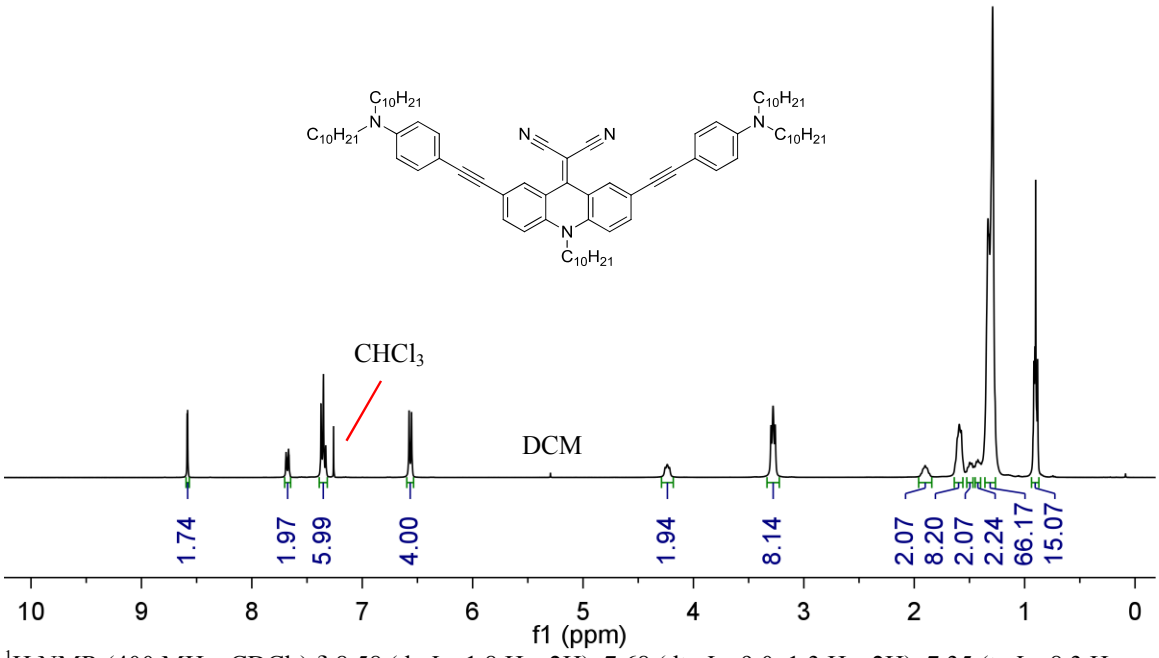

^{1}H NMR (400 MHz, $CDCl_3$) δ 8.58 (d, J = 1.8 Hz, 2H), 7.68 (dt, J = 9.0, 1.3 Hz, 2H), 7.35 (t, J = 8.3 Hz, 6H), 6.56 (d, J = 9.0 Hz, 2H), 4.39 – 4.13 (m, 2H), 3.39 – 3.20 (m, 8H), 2.08 – 1.77 (m, 2H), 1.68 – 1.53 (m, 8H), 1.53 – 1.45 (m, 2H), 1.46 – 1.38 (m, 2H), 1.39 – 1.22 (m, 66H), 1.00 – 0.81 (m, 15H).

4b

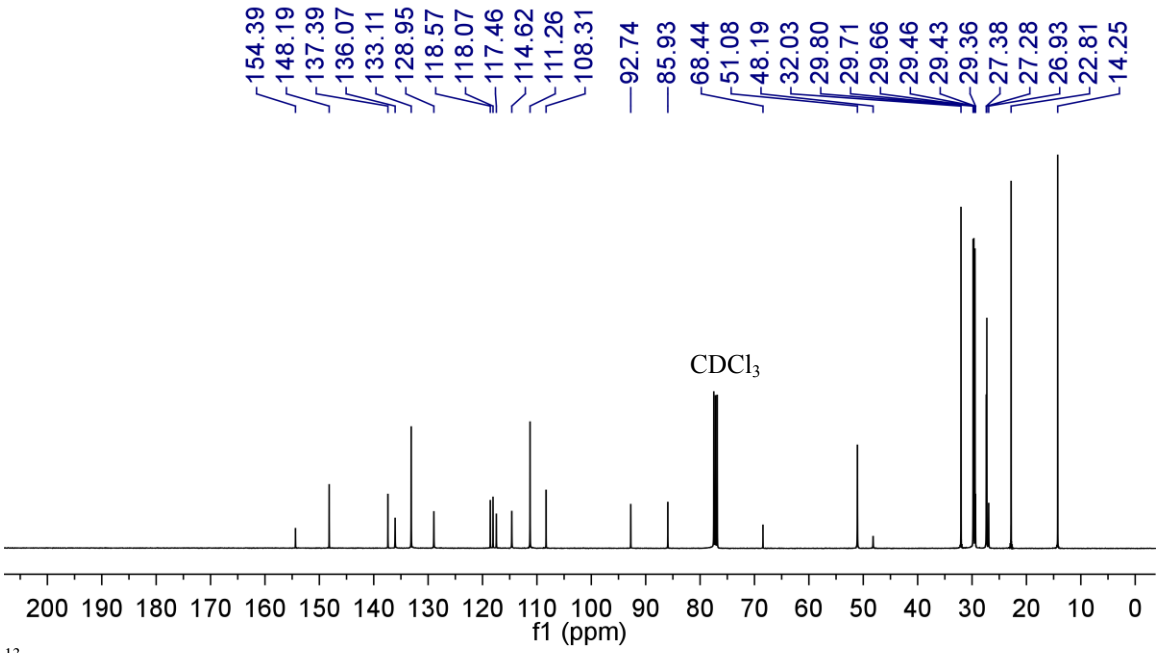

^{13}C NMR (101 MHz, $CDCl_3$) δ 154.39, 148.19, 137.39, 136.07, 133.11, 128.95, 118.57, 118.07, 117.46, 114.62, 111.26, 108.31, 92.74, 85.93, 68.44, 51.08, 48.19, 32.03, 29.80, 29.71, 29.66, 29.46, 29.43, 29.36, 27.38, 27.28, 26.93, 22.81, 14.25.

1. Catalán, J. *The Journal of Physical Chemistry B*, 2009, **113**, 5951-5960.
2. Vogt, R. A.; Gray, T. G. and Crespo-Hernández C. E. *J. Am. Chem. Soc.*, 2012, **134**, 14808–14817